



Information Technology in Medical Diagnostics

Editors:

Waldemar Wójcik and Andrzej Smolarz

 CRC Press
Taylor & Francis Group
A BALKEMA BOOK

PROCEEDINGS OF THE XIIITH CONFERENCE WD 2016, LUBLIN, POLAND, 11–13 JUNE 2016 AND THE XIIITH INTERNATIONAL CONFERENCE – MEASUREMENT AND CONTROL IN COMPLEX SYSTEMS, M^{CCS}- 2016, VINNITSIA, UKRAINE 3–6 OCTOBER 2016

Information Technology in Medical Diagnostics

Editors

Waldemar Wójcik & Andrzej Smolarz

*Electrical Engineering and Computer Science Faculty, Lublin University of Technology,
Lublin, Poland*



CRC Press

Taylor & Francis Group

Boca Raton London New York Leiden

CRC Press is an imprint of the
Taylor & Francis Group, an **informa** business

A BALKEMA BOOK

CRC Press/Balkema is an imprint of the Taylor & Francis Group, an informa business

© 2017 Taylor & Francis Group, London, UK

Typeset by V Publishing Solutions Pvt Ltd., Chennai, India
Printed and Bound by CPI Group (UK) Ltd, Croydon, CR0 4YY

All rights reserved. No part of this publication or the information contained herein may be reproduced, stored in a retrieval system, or transmitted in any form or by any means, electronic, mechanical, by photocopying, recording or otherwise, without written prior permission from the publisher.

Although all care is taken to ensure integrity and the quality of this publication and the information herein, no responsibility is assumed by the publishers nor the author for any damage to the property or persons as a result of operation or use of this publication and/or the information contained herein.

Published by: CRC Press/Balkema
Schipholweg 107C, 2316 XC Leiden, The Netherlands
e-mail: Pub.NL@taylorandfrancis.com
www.crcpress.com – www.taylorandfrancis.com

ISBN: 978-1-138-29929-0 (Hbk)
ISBN: 978-1-315-09805-0 (eBook)

vi *Table of contents*

CHAPTER 5	Subpixel edge detection and localisation based on low-frequency filtering	95
1	Introduction	95
2	Methods	96
3	Experiment	99
4	Methods for edge detection based on low-frequency filtering and analysis of previous research	101
5	Diagram of the edge detection method	102
6	Conclusions	106
CHAPTER 6	Magnetocardiographic technology for human heart investigation	107
1	Introduction	107
2	Technology of magnetocardiographic study	108
3	Principles and stages of magnetocardiographic analysis	110
4	Automatic analysis of the MCG	124
5	Conclusions	127
CHAPTER 7	Processing laser beam images using parallel-hierarchical FPGA-based transformations	129
1	Introduction	129
2	Theoretical foundations of organising parallel-hierarchical networks on the basis of functional sets	130
3	Direct parallel-hierarchical transformation	132
4	Implementation of parallel-hierarchical networks for processing laser beam spot images	134
5	Results	141
6	Conclusions	144
CHAPTER 8	The conjugated null space method of blind deconvolution	147
1	Introduction	147
2	The conjugated NS method of PSF estimation	149
3	Deconvolution optimisation	151
4	Method implementation and test examples	158
5	Conclusion	165
CHAPTER 9	Biologically motivated approach to multistage image processing	169
1	Introduction	169
2	Methods	171
3	Results	175
4	Discussion and conclusion	181
CHAPTER 10	Combined models of artificial immune systems	185
1	Artificial immune systems	185
2	Hybridisation of artificial immune systems	186
3	Canonical algorithms of artificial immune systems	187
4	The combined model of negative and clonal selection	192
5	Combined immune network and negative selection model for solving of anomaly detection problems	197
6	Using hybrid negative selection algorithm with artificial immune networks for industrial diagnostics	203
7	Conclusions	207
Author index		209

CHAPTER 3

Modified method of parallel-hierarchical network teaching based on population coding

L.I. Timchenko

State University of Transport Economy and Technologies, Kyiv, Ukraine

M. Zlepko

Vinnitsia National Technical University, Vinnitsa, Ukraine

A. Smolarz & K. Gromaszek

Lublin University of Technology, Lublin, Poland

B. Suleimenov

K.I. Satpaev Kazakh National Research Technical University, Almaty, Kazakhstan

A. Kalizhanova

Al-Farabi Kazakh National University, Almaty, Kazakhstan

1 INTRODUCTION

Absence of time-consuming operations indicates a sufficient simplicity of the computational procedure that realises the parallel hierarchical transformation, and makes it an efficient method for use in various applied areas requiring a combination of a high level of parallelism and a compact form of data representation.

A general algorithm of fast recognition of laser beam spots (LBS) images can be developed based on the proposed method of parallel-hierarchical transformation for processing dynamic images (Fig. 3.1).

This algorithm envisages a call to subroutine NetForm, a subprogram serving to construct network structures for images. A detailed description of the subroutine is shown as an algorithm (Fig. 3.2).

This subroutine performs input of the initial information to the PH network. After that, G-transformation of information takes place at all levels of the PH network.

2 THE G-TRANSFORMATION

The G-transformation is performed in the following way. The vector of the incoming image is sent to the PH network input (to input elements of first level branches of the network). A mathematical model of the parallel decomposition of the set $\mu = \{a_i\}, i = \overline{1, n}$ (Timchenko et al. 2011), used in each branch of the PH network, looks as follows:

$$\sum_{i=1}^n a_i = \sum_{j^z=1}^P \left(n - \sum_{k=0}^{j^z-1} n_k \right) (a^{j^z} - a^{j^z-1}),$$

where $a_i \neq 0$, P is the dimensionality of this set (a number of set elements) or the dimensionality of the PH network branch at its every level, $a^z, z = \overline{1, P}$ are elements of subsets consisting

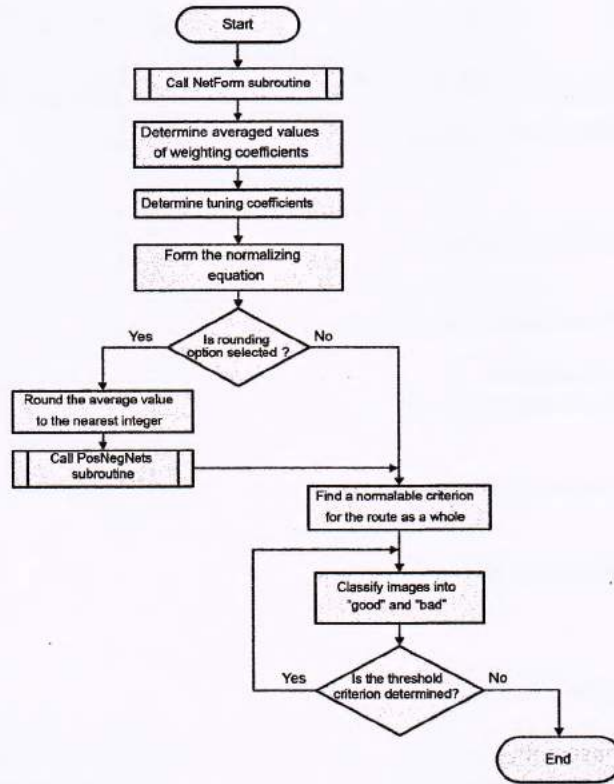


Figure 3.1 A general algorithm of laser beam spots image recognition.

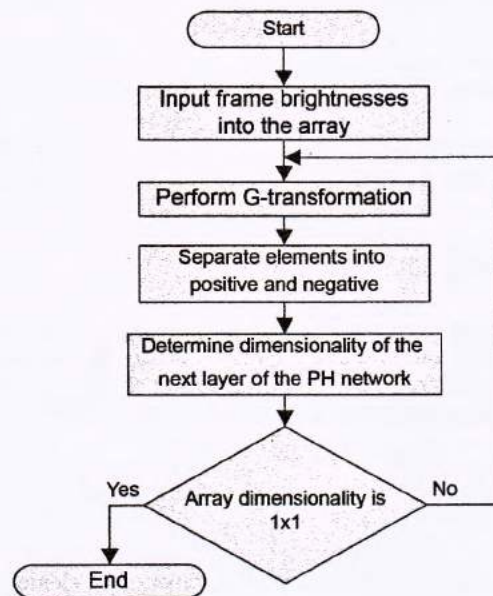


Figure 3.2 A subroutine algorithm of the creation of image network structure.

of equal elements, n_k is the number of elements in the k^{th} subset (i.e. the order of number a_j), a_j is the 1st element of the set $\{a^i\}$, selected at the j^{th} step, $j^* = 1, P, a^0 = 0, n_0 = 0$.

When a structure of two networks is constructed, the average values of weighting coefficients and tuning coefficients (2) are being determined. Based on the calculated tuning coefficients, a normalising equation (6) is being formed.

If an average value \bar{a}_i is rounded up to the nearest integer, the subroutine *PosNegNets* is called. It is a subprogram that forms two connected PH networks for processing positive and negative difference components. A formation algorithm of the two networks is similar to the formation algorithms of the network structure for images.

After that, a normalising criterion for the route as a whole is being found with further classification of images into "good" and "bad" according to the ratio.

If the threshold criterion is determined, the classification is conducted again.

Let us develop a preliminary processing algorithm of route fragments (Fig. 3.3)

An image of the laser route fragment arriving to the system input undergoes the following preliminary processing:

1. Determine maximum fragment brightness to form n border lines;
2. Having selected a necessary number of boundaries, find their geometrical centres and average parameters for the whole frame;
3. Form tunnel boundaries using a trained sample and averaged frame parameters;
4. Check if calculated frame parameters are included into the tunnel. Based on this verification, frame image classification is performed. If an image was classified as "bad", image parameters are corrected, included into the taught sample, and an additional training of the system is performed.

The developed application is intended to process and classify laser beam spots images.

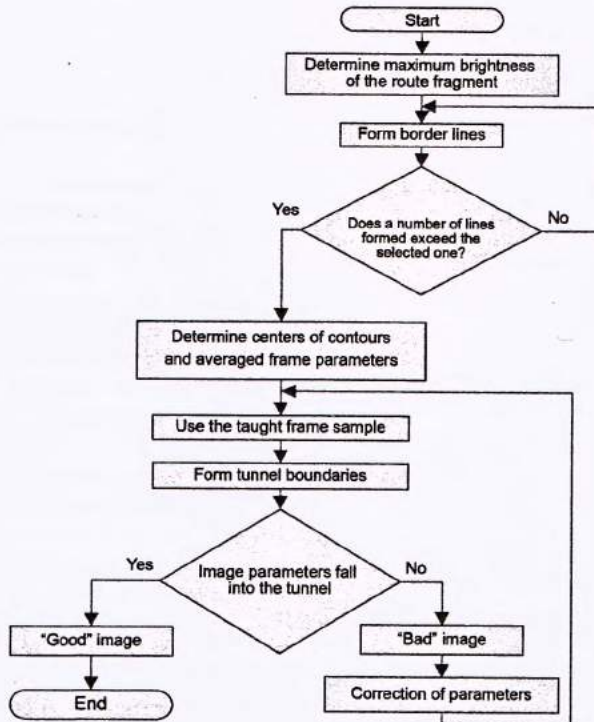


Figure 3.3 A preliminary processing algorithm of route fragments.

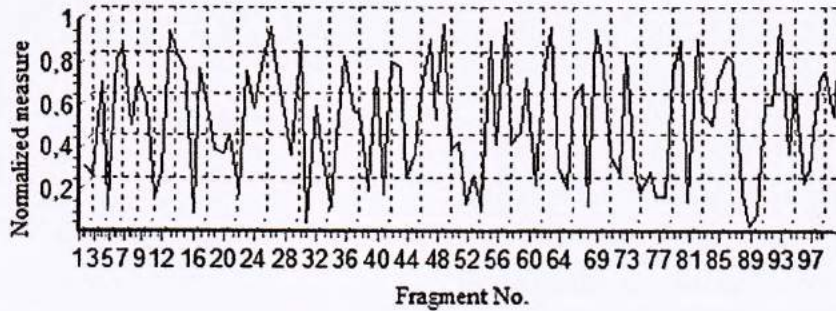


Figure 3.4 Screen form of the PH network application for fast recognition of laser beam spot images.

The software window (Fig. 3.4) represents a form divided into two parts: the left part contains a processing panel of the reference frame of the laser beam spots images route, and the right one—that of the current frame of the laser beam spots images route.

3 INFORMATION ABOUT THE FRAME PARAMETERS

Information about the frame parameters is exhibited in the upper part:

- frame width, pixels;
- frame height, pixels;
- information about the route containing the frame;
- frame file name;
- number of frames in the route.

The bottom part contains tabs:

- construction of the network graph, which can be obtained and saved as a PH network graph file;
- route fragment processing, where a route fragment can be processed;
- image comparison, where laser beam spot images are compared and classified;
- determination of energy centres, where laser beam spot energy centres are determined and the PH network is trained.

An energy centre is a point in the image, where coordinates (x, y) of a two-dimensional signal with a specific nonlinear density meet a given value of $f(x, y)$, and are expressed as follows:

$$x_{ec} = \frac{1}{M} \sum_{x=0}^{N-1} \sum_{y=0}^{N-1} w(f(x, y)) \cdot x, y_{ec} = \frac{1}{M} \sum_{x=0}^{N-1} \sum_{y=0}^{N-1} w(f(x, y)) \cdot y, M = \sum_{x=0}^{N-1} \sum_{y=0}^{N-1} w(f(x, y))$$

where M is the first order moment of inertia.

4 ESTIMATION OF EFFICIENCY

To estimate the efficiency of suggested algorithms and the soft hardware developed on their basis, let us describe the technical advantages of the means of the PH transformation as demonstrated by the developed products and conducted experiments. A comparative characterisation is shown in Table 3.1.

Table 3.1 Comparative characterisation of the means of the parallel-hierarchical transformation.

Parameter	Indices			
	Known soft hardware (imitational modelling based on MLP and RBF networks).	Known soft hardware (imitational modelling based on neural-like network technology)	Known soft hardware (CPU, PH transformation method based on the Q-decomposition)	Proposed soft hardware (GPU, method of the PH network training based on the normalising equation)
Average size of good route fragments (%)	70	74	50	18
Average value of correct recognition (%)	92	92,5	84,8	94
Accuracy of the energy centre determination, decomposition elements	1,5	1,5	1,2	0,01
Average recognition time of network processing (s)	–	–	8,4	1,52
Average time of preliminary processing of route fragments (s)	–	–	3,32	0,6

The use of neural-like network technologies for classification of extended laser route images is analysed in (Timchenko et al. 2011). The computer modelling revealed 92.5% correctly recognised images, including 74% “good” images and 60% “bad” images. In (Timchenko et al. 2011), a recognition system was modelled on the basis of the MLP neural-like network and RBF-based neural-like network. Recognition of a sample that included 140 laser route spot objects by the RBF-based neural-like network modelled in the Statistica Neural Networks 4.0 yielded 92% correctly recognised images. Comparing the results of (Timchenko et al. 2011, Timchenko et al. 2013) and those studied in this article tells us about the potential of the latter.

Therefore, the suggested method, algorithms and soft hardware permit to measure energy centre coordinates of laser route fragment images based on the normalising equation with an accuracy of no more than 0.01 decomposition elements, thus exceeding known methods (e.g. those based on determination of the gravity centre using the method of moment characteristics (Timchenko et al. 2011, Timchenko et al. 2013, Timchenko et al. 2014) by the accuracy of 1.5 times on average, which is reflected in Table 3.1. The time necessary for preliminary and network processing of the laser route fragment images decreases as well.

Four routes, each containing 100 frames, were used in experimental research of the parallel-hierarchical transformation for fast recognition of laser beam spot images. Using the normalising equation, let us determine the normalised measures for Route 1 (Fig. 3.5).

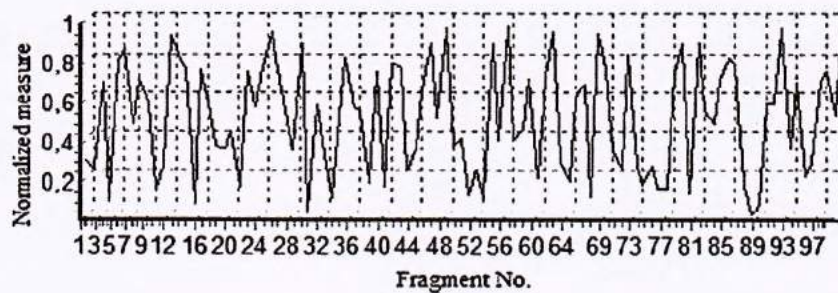


Figure 3.5 Determination of the normalised measure for further classification of Route 1 fragments.

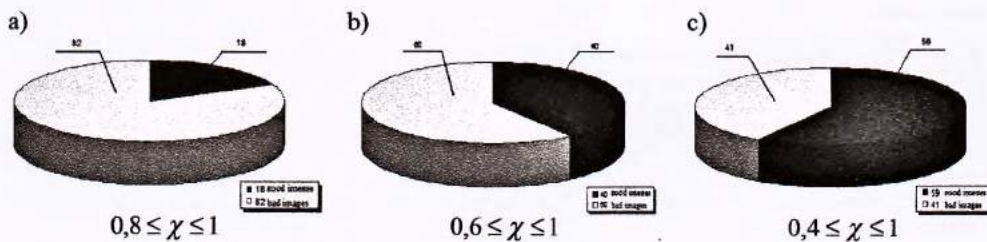


Figure 3.6 Classification of Route 1 fragments (with the respective threshold criterion).

Using inequations, let us classify images (Fig. 3.6a).

As can be seen, the portion of “good” images is 18%. As a rule, in real conditions, positions of energy centres cannot be determined absolutely accurately, therefore less tight limits should be set for the threshold criterion using relation (Figure 3.6b and 3.6c) An average portion of “good” images in this case is 40% and 59% respectively. Then the PH network is trained for repeated processing of “bad” route fragments.

In physical modelling of the method of PH transformation and determination of extended laser route image coordinates using the graphic adapter Radeon X1300, processing of a single image takes about 0.6 s. Radeon X1300 is a basic solution in the ATI Radeon family of graphic adapters based on the graphic processor RV515 with the main characteristics of 4 pixel pipelines, 4 texture units and 2 vertex pipelines.

An approach of flow programming is suggested to program the GPU. This approach includes splitting a program into relatively small stages (core programs) that process data flow elements. Core programs go into shaders, and data flows go into textures in the GPU. A shader is a program performed in the GPU and processing the data flow. “Data flow” means information about the coordinates of polygon vertices, each vertex illumination, normal mapping, texture coordinates and so on, that permanently arrives in blocks to the shader program. A video processor receives outgoing information for all three vertices of the polygon. Having data on the three vertices, the GPU goes through all the pixels of a single polygon, while gradually changing (interpolating) vertex values from one vertex to another. A shader length is a memory space of the shader program. Considering that data arriving to the shader are random for the programmer, in a sense that the order in which the data will be sent to the shader is not preset, the shader program does not have any statistical or general variables; there is nothing similar to files or information storage between calls. Otherwise, the shader program is similar to a regular C program: there are input, output and time variables, standard functions, structures, arrays, cycles and conditional operators.

Image processing takes place in the GPU with cores realised at all elements covered by the initial region. The only obvious way to calculate a scalar of the input vector is to represent 1×1 initial elements and use a core that is read in all values from the input texture. This

approach has several drawbacks. First, only one of the parallel elementary processors would be busy. Second, that would probably exceed the maximum memory size, including the memory of the shader and static instruction of calculation for some hardware. That is why we will perform a parallel operation of reduction based on global methods of communication on parallel computers.

5 EXPERIMENT

At the high level, GPU-based parallel calculation is a correction of sizes of the input and output texture and of index elements. For the presented vector M of the length M , the output of the first step is $M/2$ with texture $M/2$. For each of its elements, coordinates for input texture are corrected in such a way that they correspond to disconnected 2×2 subregions. Then the values in those subregions are compared. This is repeated recursively until the 2×2 texture is reduced finally to the 1×1 "scalar" texture through a logarithmic series of repetitions.

Next series of images finalise the first step of the 8×8 algorithm reduction of the input texture (Fig. 3.7). The left image demonstrates the input texture. Initial elements are marked in green (Fig. 3.7a). The right image is a result of the first round of reduction. Each initial element contains a local transfer maximum of the 2×2 subregion in the input texture. This relation, in addition, is distinguished in the second line of images (Fig. 3.7b). Next, let us determine the coordinates of energy centres of a fragment of Route 1 (Fig. 3.8). A diagram of changes in the energy centre coordinates of fragments of Route 1 is shown in Figure 3.9.

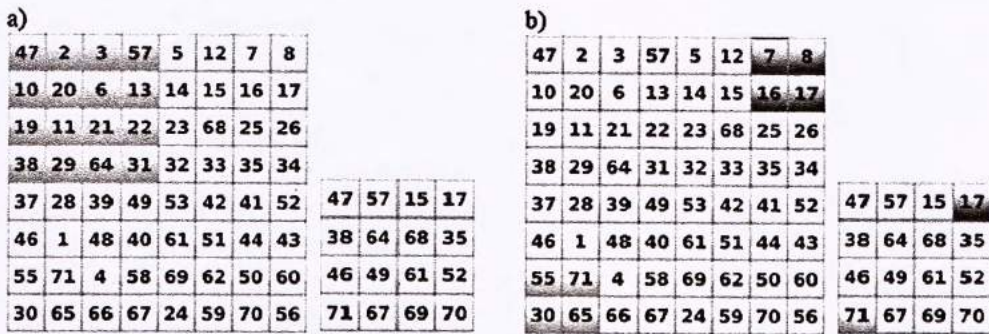


Figure 3.7 A diagram of pixel processing using the Radeon X1300 graphic adapter.

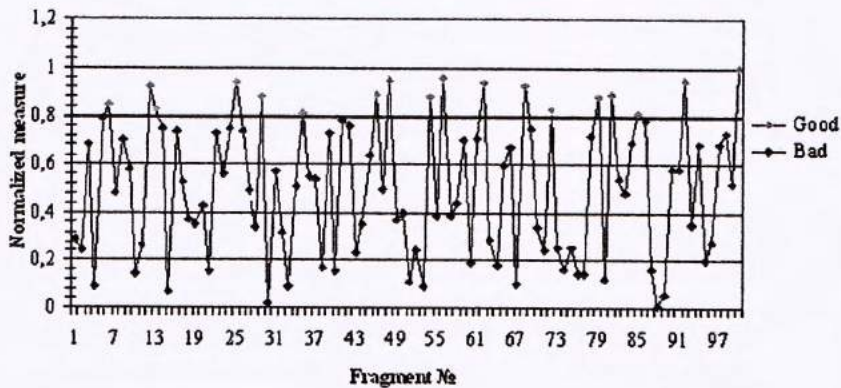


Figure 3.8 A diagram of formation of "good" and "bad" images in Route 1.

After the PH network training, a portion of “good” images was 83% (as compared to 18%). The graphic interpretation of determination of energy centre coordinates after the PH network training is demonstrated in Figure 3.10.

After the PH network training, a portion of “good” images of Route 2 was 76% (12% before training) (Fig. 3.11 versus Fig. 3.12).

After the PH network training, a portion of “good” images of fragments of Route 3 was 65% (15% before training) (Fig. 3.13 versus Fig. 3.14).

Finally, after the PH network training, a portion of “good” images of route 4 reached 83% as compared to 17% before training (Fig. 3.15 versus Fig. 3.16).

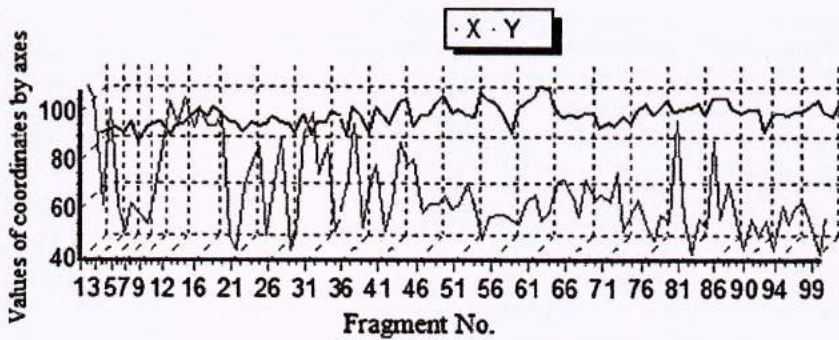


Figure 3.9 Determination of coordinates of energy centers of Route 1 fragments.

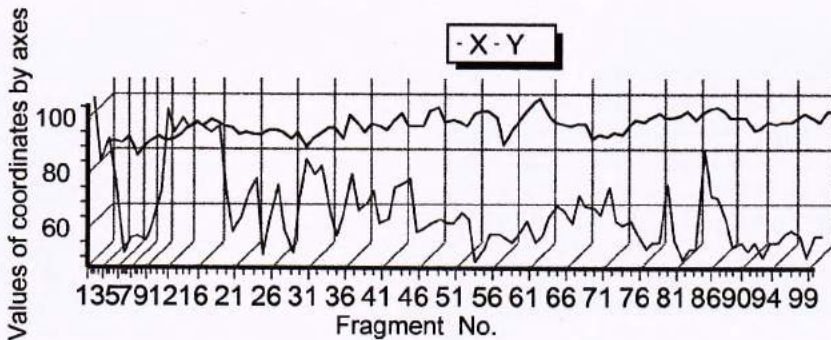


Figure 3.10 Determination of energy centre coordinates of fragments of Route 1 after the PH network training.

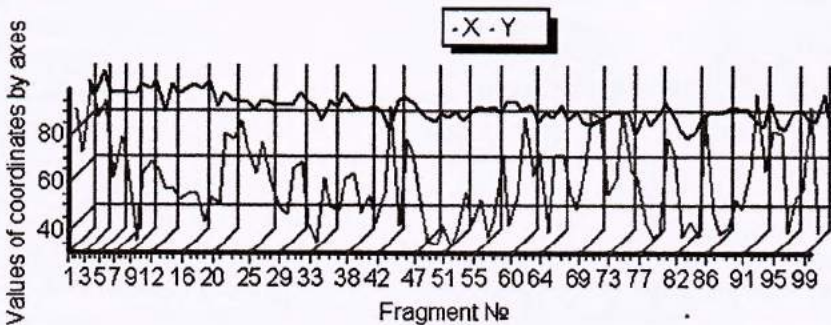


Figure 3.11 Determination of energy centre coordinates of fragments of Route 2.

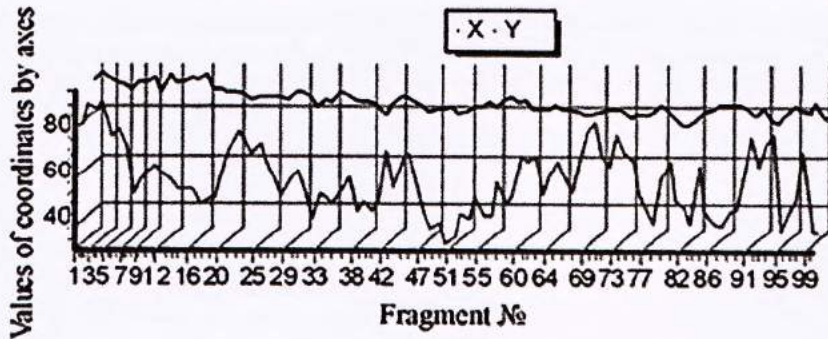


Figure 3.12 Determination of energy centre coordinates of fragments of Route 2 after the PH network training.

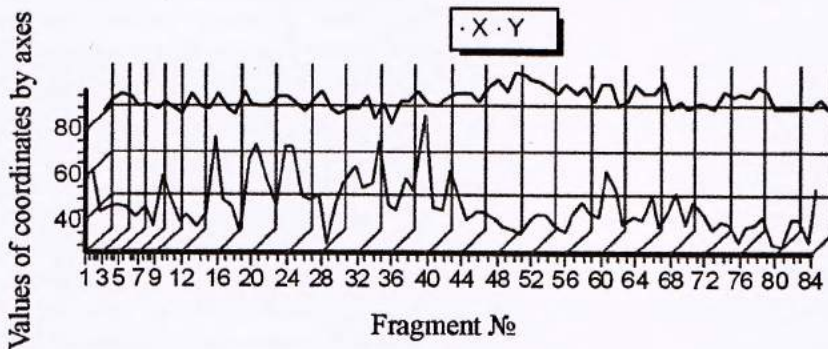


Figure 3.13 Determination of energy centre coordinates of fragments of Route 3.

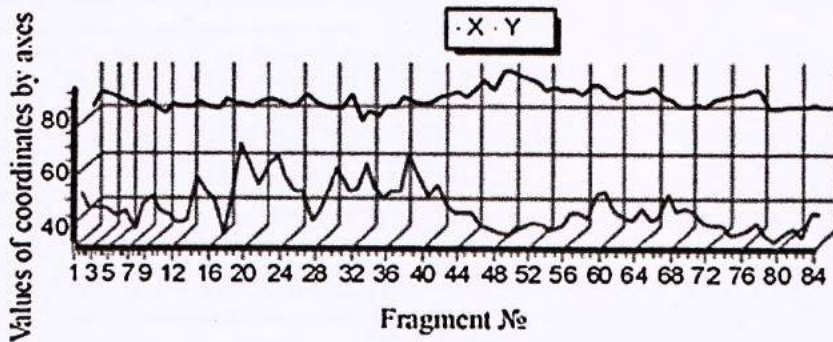


Figure 3.14 Determination of energy centre coordinates of fragments of Route 3 after the PH network training.

The work deals with an important problem of improved efficiency of dynamic image recognition. The analysis of modern trends in the development of fast recognition technologies for dynamic images, as well as the analysis of the PH transformation development, allows to classify the suggested parallel-hierarchical approach as a neural-like method of transformation with a network of direct propagation and the space-time organisation of connections.

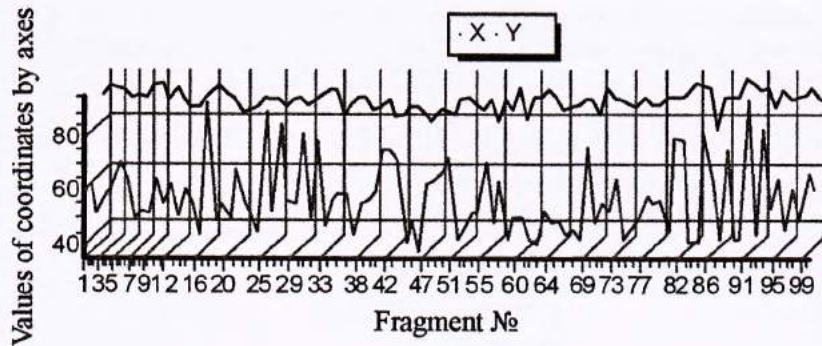


Figure 3.15 Determination of energy centre coordinates of fragments of Route 4.

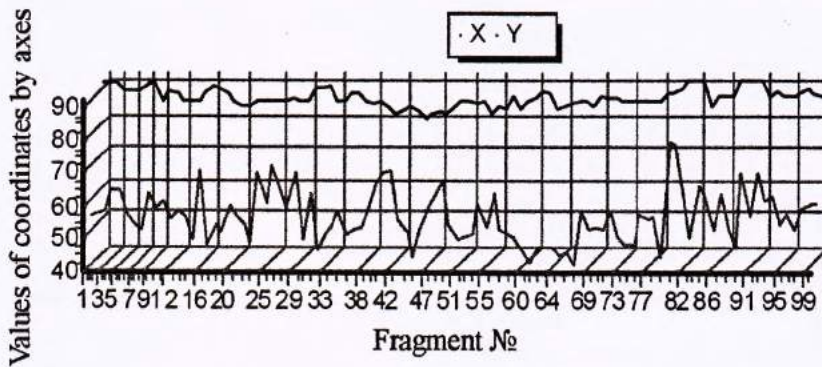


Figure 3.16 Determination of energy centre coordinates of fragments of route 4 after the PH network training.

The authors think that efficiency of computational structures can be increased by applying a developed method of PH transformation with the formation of a normalising equation.

For quality classification and processing of a sequence of extended laser route spot images, a threshold criterion was introduced. Methods of PH transformation were developed: by introducing a set A that contains measures of correspondence between the reference and current PH network tuning coefficients, and by finding a measure of correspondence between two networks as a whole.

Using a normalising equation, processing and recognition of algorithms for laser beam spot images were developed, and PH network structures for images based on G-transformation were constructed. The developed algorithms allow to determine energy centre positions and to classify laser route image frames. Peculiarities of real-time realisation of the algorithm of the developed method for route fragments are discussed, and a choice of means for software development is explained. On the basis of the developed algorithms, software was created for modelling a neural-like parallel-hierarchical network, which was used for image classification and fast processing.

Experimental methods to study the processing of laser beam spot image fragments were developed, which allow to verify the adequacy of the proposed algorithms and to obtain results of fast processing and classification of laser beam spot image fragments.

In the conducted experiments, an average portion of “good” route fragments was 17%, as compared to 50% in (Timchenko et al. 2011). However, after the training, it increased to 79.25%

(as compared to 65% (Timchenko et al. 2013)). It was also established that an average rate of correct recognition was 94% (84.8% (Timchenko et al. 2013)), and the accuracy of energy centre determination was no more than 0.01 decomposition elements (as compared to 1.2 decomposition elements (Kim & Wunsch 2003)), which is reflected in Table 3.1. This is, on average, 1.5 times higher than the accuracy of the known methods, for instance in comparison to gravity centre determination using a method of moment characteristics. Physical modelling of the PH transformation method for fast image recognition using the Radeon X1300 graphic adapter demonstrates that the processing of one image requires approximately 0.6 s (3.32 s (Timchenko et al. 2013)), and network processing requires 1.52 s (8.4 s (Timchenko et al. 2013)).

From recent achievements in the sphere of neurobiological research it is known that for coding within the frame of such an approach the information is presented by the population of active neurons (Haykin 1999, Timchenko et al. 2011). This important property was demonstrated in the experiments performed by Sparks, analysing how the brain of a monkey controls the motion of its eyes. The conclusion was made that the needed motion is coded by a population of the cells, each of which presents a motion different from others. The motion performed by the eye corresponds to the average of all the motions, coded by the active cells. As Yaung and Yamane showed in the experiments with the cerebral cortex of a monkey, population coding is valid not only for the motion of eyes but also for features of the face.

In accordance with the idea of population coding, the currently recognised image must be compared with a certain average representation of the reference pattern—average by all current patterns (in other words, by all the teaching sample) on the basis of averaging the PH network parameters.

Let us use the general idea of population coding (Timchenko et al. 2013) and construct a model of any finite operation conducted by all current operations, i.e. a finite operation consisting of a sequence of current operations. For instance, a finite operation in the form of a visual saccade consists of a sequence of current micro-saccades. At the branch level of the neural network, this finite operation with the realisation of population coding meets the averaged parameters of this network (Timchenko et al. 2013). For the PH network, both a number of elements in the branch of each level, which are determined on the basis of the model, and the values of the element itself may be taken as averaged parameters. In this case the currently recognised pattern will be reflected by the current PH network and compared with the reference PH network with averaged parameters (the PH network with averaged parameters forms a reference network of the reference pattern).

Having denoted the average value of the random element of the first level as $\bar{a}_{i,j}^1$, the second level as $\bar{a}_{i,j}^2$, the third level as $\bar{a}_{i,j}^3$, etc., the k^{th} last level as $\bar{a}_{i,j}^k$, and the average number of elements of the first level as $N_{\bar{a}_{i,j}^1}$, the second level as $N_{\bar{a}_{i,j}^2}$, the third level as $N_{\bar{a}_{i,j}^3}$, etc., and the k^{th} level as $N_{\bar{a}_{i,j}^k}$, one can form a PH network with averaged parameters according to the idea of population coding. The average number of certain layer elements is calculated according to the formula:

$$\bar{a}_{i,j}^k = \frac{\sum a_{i,j}^k}{N_{\bar{a}_{i,j}^k}}.$$

The structure of the PH network with averaged parameters thus synthesised is shown in Figure 3.17.

A current pattern or a tested pattern prepared by the parallel-hierarchical network with current parameters $a_{i,j}^1, a_{i,j}^2, a_{i,j}^3, \dots, a_{i,j}^k$ and a respective number of elements in branches of each level $N_{a_{i,j}^1}, N_{a_{i,j}^2}, N_{a_{i,j}^3}, \dots, N_{a_{i,j}^k}$ is being compared with the reference pattern prepared by the parallel-hierarchical network with averaged parameters $\bar{a}_{i,j}^1, \bar{a}_{i,j}^2, \bar{a}_{i,j}^3, \dots, \bar{a}_{i,j}^k$ and an average number of elements in branches of the respective level $N_{\bar{a}_{i,j}^1}, N_{\bar{a}_{i,j}^2}, N_{\bar{a}_{i,j}^3}, \dots, N_{\bar{a}_{i,j}^k}$. Current parallel-hierarchical network parameters $a_{i,j}^1, a_{i,j}^2, a_{i,j}^3, \dots, a_{i,j}^k$ are calculated in network branches.

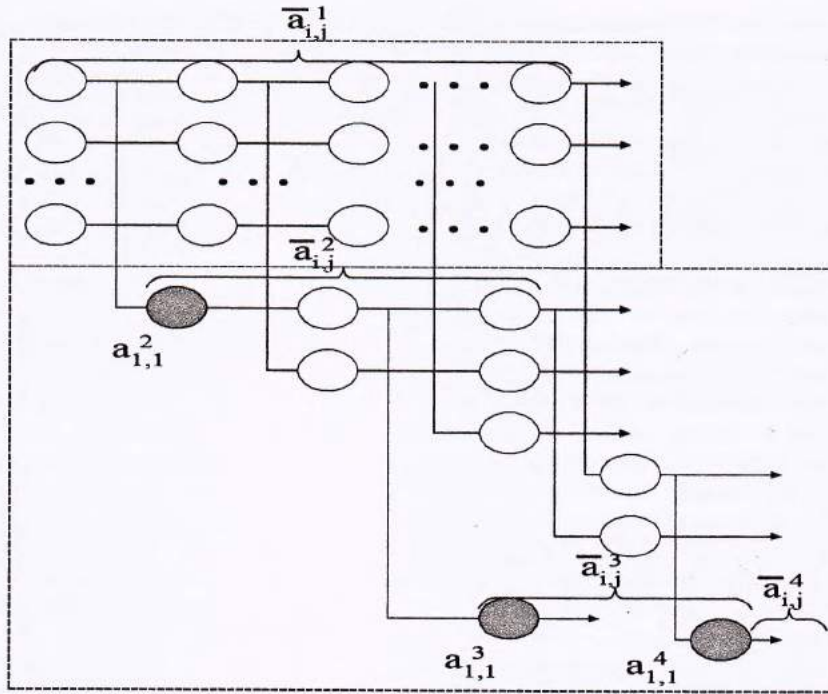


Figure 3.17 Structure of the parallel-hierarchical network with averaged parameters.

A current pattern or a tested pattern prepared by the parallel-hierarchical network with current parameters $a_{i,j}^1, a_{i,j}^2, a_{i,j}^3, \dots, a_{i,j}^k$ and a respective number of elements in branches of each level $N_{a_{i,j}^1}, N_{a_{i,j}^2}, N_{a_{i,j}^3}, \dots, N_{a_{i,j}^k}$ is being compared with the reference pattern prepared by the parallel-hierarchical network with averaged parameters $\bar{a}_{i,j}^1, \bar{a}_{i,j}^2, \bar{a}_{i,j}^3, \dots, \bar{a}_{i,j}^k$ and an average number of elements in branches of the respective level $N_{\bar{a}_{i,j}^1}, N_{\bar{a}_{i,j}^2}, N_{\bar{a}_{i,j}^3}, \dots, N_{\bar{a}_{i,j}^k}$. Current parallel-hierarchical network parameters $a_{i,j}^1, a_{i,j}^2, a_{i,j}^3, \dots, a_{i,j}^k$ are calculated in network branches.

Using an adaptive threshold transformation with a computed threshold based on a formula for boundary preparation of the parallel-hierarchical network elements for each level as described in (Timchenko et al. 2013), and on the basis of the three-level coding, it is possible to represent averaged parameters $\bar{a}_{i,j}^1, \bar{a}_{i,j}^2, \bar{a}_{i,j}^3, \dots, \bar{a}_{i,j}^k$ with their ternary labels (-1, 0, +1). Then arrays of difference of the element with an average brightness value of decomposition elements of the pattern (or of its fragment) are determined.

For a random averaged parameter, a ternary level transition may be presented by three types of labels: zero label $a_{i,j}^0$, positive $a_{i,j}^1$, and negative $a_{i,j}^{-1}$. In this case a parallel-hierarchical network with numerical counts is transformed into a parallel-hierarchical network with counts $a_{i,j}^0, a_{i,j}^1, a_{i,j}^{-1}$ (Timchenko et al. 2011). This ternary transformation procedure may be described in the following form:

$$R_{i,j} = a_{i,j}^k - \bar{a}_{i,j}^k.$$

To prepare a pattern, the resulting difference is compared with the computed threshold δ , i.e.

$$a_{i,j}^{(\cdot)} = \begin{cases} 1, & \text{if } R_{i,j} > \delta \\ -1, & \text{if } R_{i,j} < -\delta. \\ 0, & \text{if } |R_{i,j}| \leq \delta \end{cases} \quad (3.1)$$

The threshold δ is calculated from the condition:

$$N_i^{(1)} \cdot N_i^{(-1)} \cdot N_i^{(0)} = \text{Max}, \quad (3.2)$$

When condition (3.2) is satisfied, the relation $N_i^{(1)} \approx N_i^{(-1)} \approx N_i^{(0)}$ will be true.

In contrast to the threshold transfer function of a neuron for the known neural networks (Haykin 1999), when a parallel-hierarchical network is realised for the threshold function (3.1), a threshold is not set as a certain constant, but is a function of a number of positive, negative and zero preparations, and is calculated by (3.2).

Therefore, the threshold adaptive transformation ensures that when forming ternary labels, current and averaged image elements are not compared at the level of noise signals, or with zero, in (3.1). Instead, for each image its own threshold δ is calculated that would be adapted to a particular image, thus increasing noise immunity of the transformation.

Such a transformation simplifies the correlation comparison procedure of current and reference parallel-hierarchical network counts, because it is performed on simple labels (0, +1, -1) instead of halftone counts.

In order to form reference images, training within a sample should be conducted. For this purpose, it is necessary to perform averaging in branches of each level, i.e. to form averaged elements $\bar{a}_{i,j}^1, \bar{a}_{i,j}^2, \bar{a}_{i,j}^3, \dots, \bar{a}_{i,j}^k$ and then move to ternary labels $a_{i,j}^0, a_{i,j}^1, a_{i,j}^{-1}$. Having completed the manipulations described above, it is possible to form a parallel-hierarchical network with reference parameters for current images. After that a correlation coefficient of the parallel-hierarchical network with current parameters can be found. (Under the parallel-hierarchical network with current parameters we understand a PH network with current values of its elements $a_{i,j}^1, a_{i,j}^2, a_{i,j}^3, \dots, a_{i,j}^k$ with a transfer to ternary labels $a_{i,j}^0, a_{i,j}^1, a_{i,j}^{-1}$ and a current number of elements in the branch of each level $N_{a_{i,j}^1}, N_{a_{i,j}^2}, N_{a_{i,j}^3}, \dots, N_{a_{i,j}^k}$).

To analyse the data when their sequence is important, time series are used. In this method, coordinates of energy centres of laser beam spot images are used as estimates of interest.

That is, for a random average parameter such a transition can be presented by three kinds of preparations: $a_{i,j}^0, a_{i,j}^1$ and $a_{i,j}^{-1}$. In this case, a parallel-hierarchical network with numerical counts will be transformed into a PH network with binarised counts $a_{i,j}^0, a_{i,j}^1$ and $a_{i,j}^{-1}$. As a result, the comparison procedure of binarised counts of current and reference PH networks is considerably simplified.

For the formation of referenced image, for instance of a biomedical image of the norm and images with pathologies, it is necessary to carry out their teaching within the limits of the teaching sample.

For this purpose it is necessary, during each teaching stage, to make an average by the element of the branch of each level, i.e. from average elements $\bar{a}_{i,j}^1, \bar{a}_{i,j}^2, \bar{a}_{i,j}^3, \dots, \bar{a}_{i,j}^k$ further passing to the binarised preparations $a_{i,j}^0, a_{i,j}^1, a_{i,j}^{-1}$. Having performed the above-mentioned actions, PH networks can be formed with reference parameters for the images of the form and images with various pathologies.

Having realised parallel-hierarchical networks with reference parameters for normal images and images with various pathologies, a comparison with the parallel-hierarchical network can be made, using current parameters. By the PH network with current parameters we imply the parallel-hierarchical network with current values of its elements $a_{i,j}^1, a_{i,j}^2, a_{i,j}^3, \dots, a_{i,j}^k$ with the transition to the binarised preparations $a_{i,j}^0, a_{i,j}^1, a_{i,j}^{-1}$ and the current number of elements in the branches of each level $N_{a_{i,j}^1}, N_{a_{i,j}^2}, N_{a_{i,j}^3}, \dots, N_{a_{i,j}^k}$. The comparison procedure of the parallel-hierarchical network with reference parameters and the PH network with current parameters comprises their topographic superposition and calculation of the number of coincidences of the same binarised elements.

Two binarised PH networks coincide if all the counts of each preparation similarly located in the network are pairwise equal. In case of detergency dimensionalities of the compared parallel-hierarchical networks it is necessary to introduce in its branches additional codes with coding of the fourth state. For evaluation of the result of binarised parallel-hierarchical networks we will introduce a quantitative index, characterising their degree of coincidence (3.3)

$$R(c_e, c_n) = \sum (a_{i,j}^{1(\dots)})_e \cap (a_{i,j}^{1(\dots)})_n + \dots + \sum (a_{i,j}^{k(\dots)})_e \cap (a_{i,j}^{k(\dots)})_n, \quad (3.3)$$

where $c_e = f_e(a_{i,j}^1, a_{i,j}^2, \dots, a_{i,j}^k)$ is the networking function of a reference image, $c_n = f_n(a_{i,j}^1, a_{i,j}^2, \dots, a_{i,j}^k)$ is the networking function of the current image and $a_{i,j}^{k(\dots)} \in \{a_{i,j}^{k(0)}, a_{i,j}^{k(1)}, a_{i,j}^{k(-1)}\}$, and \cap denotes a coincidence of similar binarised preparations, when they are compared. Components (3.3) equal unit only in the case, when similar preparations coincide, i.e.:

$$(a_{i,j}^{k(\dots)})_e \cap (a_{i,j}^{k(\dots)})_n = \begin{cases} 1, & \text{if } (\dots) = (\dots) \\ 0, & \text{else} \end{cases}$$

The total number of the elements in the reference PH network is calculated in the following manner

$$N_e = N_{a_{i,j}^1} + N_{a_{i,j}^2} + \dots + N_{a_{i,j}^{k-1}} + N_{a_{i,j}^k}$$

Normalised degree of binarised preparations comparison is calculated in the following way:

$$\mathfrak{R} = \frac{R(c_e, c_n)}{N_e}$$

We suggest the following example of binarised preparations comparison at the second level for two PH networks (Fig. 3.18).

Let us calculate for this example (Fig. 3.18) the degree of coincidence $R(c_e, c_n)$ and the normalised degree of comparison \mathfrak{R} for the second level of the current and reference PH networks.

$$R(c_e, c_n) = (1) + (1+1) + (1+1) + (1+1+1) + (1+1+1+1) + (1+1+1+1) = 16.$$

The total number of elements in the reference PH network at the second level is $N_e = 21$. The normalised degree of comparison \mathfrak{R} while comparing the binarised counts of the current and reference PH networks for their other levels will be the following:

$$\mathfrak{R} = \frac{R(c_e, c_n)}{N_e} = \frac{16}{21} \approx 0,762$$

It is obvious that the normalised measure of comparison of two PH networks is defined within the following limits

$$0 \leq \mathfrak{R} \leq 1.$$

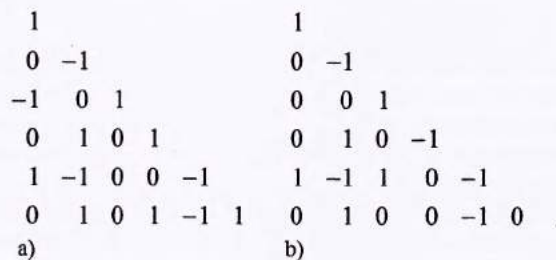


Figure 3.18 Example of the comparison of binarised preparations at the second level of: a) the reference PH network, and b) the current PH network.

6 CONCLUSIONS

An important factor is that the normalised measure of comparison can be calculated not only separately for each two levels, but also in common for two PH networks. This improves the probability of the recognition of results formation. Thus, for network teaching, we suggest applying the idea of population coding in an artificial neural network and its similarity to natural neural networks, to represent the current image by the current PH network with current parameters and transform it on the basis of generalised content preparation into a binarised preparation, with further comparison on the basis of the normalised measure of comparison with the reference PH network of a reference pattern having average parameters, elements of which are binarised preparations. Unlike the known structures of artificial neural networks, where non-normalised (absolute) similarity criteria are used for comparison, in the considered method of teaching a normalised criterion is used. A normalised measure of comparison is suggested not only for separate calculations for each of the two levels, but also for joint calculations for each level of PH networks. This improves the accuracy of the recognition of results formation.

REFERENCES

- Haykin S. 1999. *Neural Networks*. New Jersey: Prentice Hall.
- Kim, S. & Wunsch, D.C. 2003. A GPU based parallel hierarchical fuzzy ART clustering. *Proc IJCNN*: 2778–2782.
- Timchenko, L.I., Melnikov, V.V., and Kokryatskaya, N.I. 2011. Method of parallel-hierarchic organization of network for proceeding of image. *Cybernetic and System Analysis* 47(1):140–151.
- Timchenko, L.I., Kokryatskaya, N.I. and Shpakovych V.V. 2013. Modeling of a method of parallel hierarchical transformation for fast recognition of dynamic images. *EURASIP Journal on Advances in Signal Processing* 2013:87.
- Timchenko, L., Kutayev, Y., Cheporniuk, S., Kokriatskaya, N., Yarovy, A. and Denysova, A. 2014. A new approach to detection of noise-distorted signals based on the method of S-preparation. *Journal of IET Image Processing* 8(11): 627–638.

Table of contents

Preface	vii
About the editors	ix
CHAPTER 1 Recognition of textured objects using optimal inverse resonant filtration	1
1 Introduction	1
2 Object recognition problem statement as the problem of optimal filtration	4
3 Harmonic model of textured image	6
4 Design of optimal inverse resonant filter	8
5 Creation of functions basis for eigen harmonic decomposition	13
6 Implementation and experimental analysis of the IRF	18
7 Conclusions	23
CHAPTER 2 Approximation of bidirectional reflectance distribution function for highly efficient shading	27
1 Introduction	27
2 Analysis of existing approaches to BRDF approximation and problem formulation	27
3 Approximation of BRDF by the 3-degree polynomial	29
4 Approximation of BRDF by using logarithmic function	31
5 BRDF approximation models based on new cosine-degree functions with simple hardware implementation	34
6 A method for accelerated computation of color intensities for scan-line fills of three-dimensional graphics objects	39
7 Conclusions	46
CHAPTER 3 Modified method of parallel-hierarchical network teaching based on population coding	49
1 Introduction	49
2 The G-transformation	49
3 Information about the frame parameters	52
4 Estimation of efficiency	52
5 Experiment	55
6 Conclusions	63
CHAPTER 4 Methods and systems of 2D polarization multi-matrix tomography of birefringent biological tissues and fluids	65
1 Introduction	65
2 Materials and methods of 2D polarization Mueller-matrix tomography	66
3 Metrological characteristics of measurement errors distributions in the system of Mueller-matrix mapping of biological layers	81
4 Diagnostic possibilities of orientation and phase Mueller-matrix tomography of polycrystal networks of blood plasma	85
5 Conclusions	92

Author index

- Akhmetov, B. 1, 169
Amirgalijev, E. 95
- Bilynsky, Y.Y. 95
Bunyak, Y.A. 1, 147
Burlibay, A. 27, 65
- Gromaszek, K. 49
- Ivasyuk, I.D. 169
- Junisbekov, M. 95, 185
- Kalimoldayev, M. 27
Kalizhanova, A. 49, 147
Kisala, P. 95, 129
Kokryatskaya, N.I. 129, 169
Komada, P. 27, 147
Kotyra, A. 1, 95
Kvyetnyy, R.N. 1, 147
- Lytvynenko, V.I. 185
- Małecka-Massalska, T. 65, 169
- Nedayvoda, I.V. 107
- Omiotek, Z. 65, 169
Orshubekov, N.A. 65, 147
- Pavlov, S.V. 27, 65
Petrovskiy, N.S. 129
Primin, M.A. 107
- Ratushny, P.M. 95
Romaniuk, R. 129
Romanyuk, O.N. 27
Romanyuk, S.O. 27
- Sikora, J. 27
Smailova, S. 129
Smolarz, A. 49, 107, 185
Sofina, O.Yu. 1, 147
Suleimenov, B. 49, 107, 185
Surtel, W. 107
- Timchenko, L.I. 49, 129, 169
Tymchuk, S.V. 27
- Wójcik, W. 1, 147, 185
- Yarovy, A.A. 129
- Zabolotna, N.I. 65
Zlepko, M. 49